Research Article | Vol. 7, No. 2 | 1 Feb 2017 | OPTICAL MATERIALS EXPRESS 569

Optical Materials EXPRESS

Tunable unidirectional surface plasmon polariton launcher utilizing a graphene-based single asymmetric nanoantenna

LEI HUANG,[1] SHAN WU,[2] YULIN WANG,[2] XIANGJUN MA,[1] HONGMEI DENG,[1] SHUMING WANG,[2] YE LU,[1] CHUANQI LI,[1,3] AND TAO LI,[2,4]

[1]*Lab of Optoelectronics and Optical Communications, Department of Electronic Engineering, Guangxi Normal University, Guilin, Guangxi 541004, China*
[2]*National Laboratory of Solid State Microstructures, College of Engineering and Applied Sciences, Nanjing University, Nanjing 210093, China*
[3]*lcq@mailbox.gxnu.edu.cn*
[4]*taoli@nju.edu.cn*

Abstract: We design and numerically investigate a graphene-based asymmetric nanoantenna microstructure that can be used to realize electrically controllable, unidirectionally propagating broadband surface plasmon polaritons. The device geometry facilitates the simultaneous excitation of two localized surface plasmons resonances in the whole structure, and consequently, the asymmetric nanoantenna can be considered as being composed of two oscillating magnetic dipoles, wherein the interference of the radiated electromagnetic waves leads to a unidirectional propagation effect. Our results indicate that our proposed active device is promising for realizing compactable, tunable, terahertz plasmonic light sources.

OCIS codes: (240.6680) Surface plasmons; (240.0310) Thin films; (260.5740) Resonance; (350.5030) Phase.

References and links

1. J. A. Schuller, E. S. Barnard, W. Cai, Y. C. Jun, J. S. White, and M. L. Brongersma, "Plasmonics for extreme light concentration and manipulation," Nat. Mater. **9**(3), 193–204 (2010).
2. P. Genevet, J. Lin, M. A. Kats, and F. Capasso, "Holographic detection of the orbital angular momentum of light with plasmonic photodiodes," Nat. Commun. **3**, 1278 (2012).
3. S. Wu, Z. Zhang, Y. Zhang, K. Zhang, L. Zhou, X. Zhang, and Y. Zhu, "Enhanced rotation of the polarization of a light beam transmitted through a silver film with an array of perforated S-shaped holes," Phys. Rev. Lett. **110**(20), 207401 (2013).
4. L. Li, T. Li, X. M. Tang, S. M. Wang, Q. J. Wang, and S. N. Zhu, "Plasmonic polarization generator in well-routed beaming," Light Sci. Appl. **4**(9), e330 (2015).
5. Q. Gan, B. Guo, G. Song, L. Chen, Z. Fu, Y. J. Ding, and F. J. Bartoli, "Plasmonic surface-wave splitter," Appl. Phys. Lett. **90**(16), 161130 (2007).
6. Q. Gan, Z. Fu, Y. J. Ding, and F. J. Bartoli, "Bidirectional subwavelength slit splitter for THz surface plasmons," Opt. Express **15**(26), 18050–18055 (2007).
7. J. J. Chen, Z. Li, S. Yue, and Q. H. Gong, "Efficient unidirectional generation of surface plasmon polaritons with asymmetric single-nanoslit," Appl. Phys. Lett. **97**, 04113 (2010).
8. D. Li, D. H. Zhang, C. Yan, T. Li, Y. Wang, Z. Xu, J. Wang, and F. Qin, "Unidirectional surface plasmon-polariton excitation by a compact slot partially filled with dielectric," Opt. Express **21**(5), 5949–5956 (2013).
9. J. Yang, S. Zhou, C. Hu, W. Zhang, X. Xiao, and J. Zhang, "Broadband spin-controlled surface plasmon polariton launching and radiation via L-shaped optical slot nanoantennas," Laser Photonics Rev. **8**(4), 590–595 (2014).
10. Y. Liu, S. Palomba, Y. Park, T. Zentgraf, X. Yin, and X. Zhang, "Compact magnetic antennas for directional excitation of surface plasmons," Nano Lett. **12**(9), 4853–4858 (2012).
11. L. Wang, T. Li, L. Li, W. Xia, X. G. Xu, and S. N. Zhu, "Electrically generated unidirectional surface plasmon source," Opt. Express **20**(8), 8710–8717 (2012).
12. T. Liu, Y. Shen, W. Shin, Q. Zhu, S. Fan, and C. Jin, "Dislocated double-layer metal gratings: an efficient unidirectional coupler," Nano Lett. **14**(7), 3848–3854 (2014).
13. S. Xiao, F. Zhong, H. Liu, S. Zhu, and J. Li, "Flexible coherent control of plasmonic spin-Hall effect," Nat. Commun. **6**, 8360 (2015).
14. J. Lin, J. P. B. Mueller, Q. Wang, G. Yuan, N. Antoniou, X. C. Yuan, and F. Capasso, "Polarization-controlled tunable directional coupling of surface plasmon polaritons," Science **340**(6130), 331–334 (2013).
15. I. P. Radko, S. I. Bozhevolnyi, G. Brucoli, L. Martín-Moreno, F. J. García-Vidal, and A. Boltasseva, "Efficient unidirectional ridge excitation of surface plasmons," Opt. Express **17**(9), 7228–7232 (2009).

#281660 http://dx.doi.org/10.1364/OME.7.000569
Journal © 2017 Received 28 Nov 2016; revised 3 Jan 2017; accepted 10 Jan 2017; published 25 Jan 2017

Optical Materials EXPRESS

16. A. Pors, M. G. Nielsen, T. Bernardin, J. C. Weeber, and S. I. Bozhevolnyi, "Efficient unidirectional polarization controlled excitation of surface plasmon polaritons," Light Sci. Appl. **3**(8), e197 (2014).
17. M. Tymchenko, A. Y. Nikitin, and L. Martín-Moreno, "Faraday rotation due to excitation of magnetoplasmons in graphene microribbons," ACS Nano **7**(11), 9780–9787 (2013).
18. C. Chen, S. Rosenblatt, K. I. Bolotin, W. Kalb, P. Kim, I. Kymissis, H. L. Stormer, T. F. Heinz, and J. Hone, "Performance of monolayer graphene nanomechanical resonators with electrical readout," Nat. Nanotechnol. **4**(12), 861–867 (2009).
19. T. J. Echtermeyer, S. Milana, U. Sassi, A. Eiden, M. Wu, E. Lidorikis, and A. C. Ferrari, "Surface plasmon polariton graphene photodetectors," Nano Lett. **16**(1), 8–20 (2016).
20. T. Mueller, F. N. Xia, and P. Avouris, "Graphene photodetectors for high-speed optical communications," Nat. Photonics **4**(5), 297–301 (2010).
21. M. Liu, X. Yin, E. Ulin-Avila, B. Geng, T. Zentgraf, L. Ju, F. Wang, and X. Zhang, "A graphene-based broadband optical modulator," Nature **474**(7349), 64–67 (2011).
22. M. Liu, X. Yin, and X. Zhang, "Double-layer graphene optical modulator," Nano Lett. **12**(3), 1482–1485 (2012).
23. Y. J. Bao, S. Zu, Y. F. Zhang, and Z. Y. Fang, "Active Control of Graphene-Based Unidirectional Surface Plasmon Launcher," ACS Photonics **2**(8), 1135–1140 (2015).
24. M. D. He, K. J. Wang, L. Wang, J. B. Li, J. Q. Liu, Z. R. Huang, L. L. Wang, L. Wang, W. D. Hu, and X. S. Chen, "Graphene-based terahertz tunable plasmonic directional coupler," Appl. Phys. Lett. **105**(8), 081903 (2014).
25. A. Vakil and N. Engheta, "Transformation optics using graphene," Science **332**(6035), 1291–1294 (2011).
26. W. Gao, J. Shu, C. Qiu, and Q. Xu, "Excitation of plasmonic waves in graphene by guided-mode resonances," ACS Nano **6**(9), 7806–7813 (2012).
27. L. Zhu, Y. H. Fan, S. Wu, L. Z. Yu, K. Y. Zhang, and Y. Zhang, "Electrical control of terahertz polarization by graphene microstructure," Opt. Commun. **346**, 120–123 (2015).
28. M. Jablan, H. Buljan, and M. Soljačić, "Plasmonics in graphene at infrared frequencies," Phys. Rev. B **80**(24), 245435 (2009).
29. J. D. Jackson, *Classical Electromagnetics*, 3rd ed.; John Wiley & Sons: New York, 1999.
30. L. Zhou, C. P. Huang, S. Wu, X. G. Yin, Y. M. Wang, Q. J. Wang, and Y. Y. Zhu, "Enhanced optical transmission through metal-dielectric multilayer gratings," Appl. Phys. Lett. **97**(1), 011905 (2010).
31. J. Yang, X. Xiao, C. Hu, W. Zhang, S. Zhou, and J. Zhang, "Broadband surface plasmon polariton directional coupling via asymmetric optical slot nanoantenna pair," Nano Lett. **14**(2), 704–709 (2014).
32. Y. Yao, M. A. Kats, P. Genevet, N. Yu, Y. Song, J. Kong, and F. Capasso, "Broad electrical tuning of graphene-loaded plasmonic antennas," Nano Lett. **13**(3), 1257–1264 (2013).
33. L. Huang, Y. H. Fan, S. Wu, and L. Z. Yu, "Giant asymmetric transmission and optical rotation of a three-dimensional metamaterial," Chin. Phys. Lett. **32**(9), 094101 (2015).
34. C. Q. Li, L. Huang, W. Y. Wang, X. J. Ma, S. B. Zhou, and Y. H. Jiang, "Electromagnetically induced transparency in nano-structures made from metallic nanorod and split-ring-resonator," Opt. Commun. **355**, 337–341 (2015).
35. S. Wu, Q. J. Wang, X. G. Yin, J. Q. Li, D. Zhu, S. Q. Liu, and Y. Y. Zhu, "Hybridized effects of plasmonic quadrupolar and dipolar resonances on the perforated planar metallic film," Appl. Phys. Lett. **93**, 101113 (2008).
36. E. Prodan, C. Radloff, N. J. Halas, and P. Nordlander, "A hybridization model for the plasmon response of complex nanostructures," Science **302**(5644), 419–422 (2003).

1. Introduction

Surface plasmon polaritons (SPPs) are the electromagnetic waves traveling along metal–dielectric or metal–air interfaces that originate from the interaction between light and collective electron oscillations on metal surfaces. SPPs have attracted considerable attraction in terms of their application to subwavelength-optics microscopy, lithography beyond the diffraction limit, and miniaturized photonics devices for practical applications. Owing to their characteristics of localized field enhancement and subwavelength confinement, SPPs have been widely applied in plasmonic metamaterial and metasurface applications [1–4]. In this context, the generation of high-efficiency unidirectional plasmon waves has formed a fundamental research issue in the area of the nano-optics, since such generation is vital to realize novel nanoscale optical devices. Researchers have previously realized unidirectional SPP devices by adding two optimized grating structures (waveguides) on the opposite sides of a slit, wherein the confined SPP propagation behavior can be analyzed in the terms of the SPP dispersion curves [5,6]. Subsequently, asymmetric slits [7,8], holes [9], nanoantennas [10], tilted gratings [11], and dislocated double-layer gratings [12] based on the interference effect have been proposed for unidirectional SPP excitation. However, unidirectional devices generally need the fabrication of precise samples to satisfy the interference-effect conditions. Constraints within current nanofabrication technologies make it difficult to construct precise

Optical Materials EXPRESS

samples in experiments. Fortunately, it is possible to solve these problems through tailoring of the phase of the radiated electromagnetic (EM) waves by methods offering external control, such as those utilizing the spin-Hall effect [13,14], and those involving changing the polarization angle of incident light [15,16].

Graphene, a single layer of carbon atoms arranged in a honeycomb lattice, exhibits almost all the electrical properties and functions required for integrated photonic circuits [17,18]. Because of high carrier mobility and wideband absorption, graphene can be potentially applied in ultrafast broadband photodetectors [19,20]. More importantly, the Fermi level of graphene depends on the bias or chemical doping, and thus, interband transitions can be switched on or off by shifting the Fermi level above or below the threshold value ($\hbar\omega/2$). Via tuning of the interband and intraband transitions, graphene can be utilized in designing for electro-optic modulators [21,22]. In this regard, tunable graphene-based unidirectional devices have recently been proposed by Fang [23] and He [24]. However, these devices offer limited scope for integration due to their structural complexity. Thus, in this study, we design a graphene-based unidirectional SPP device composed of a single asymmetric antenna and Au/SiO_2 substrate. When compared with previously proposed devices, our designed structure can achieve the tuning unidirectional SPP propagation over a broadband wavelength range based on the interference of excited localized surface plasmons (LSPs).

2. Model and simulation

Figure 1 depicts the schematic of our proposed device. An asymmetric plasmonic antenna deposited on a graphene sheet is separated from a gold substrate by a 100-nm -thick SiO_2 spacer layer. The asymmetric plasmonic antenna is composed of three different metal strips with two non-identical cavities. The geometric parameters of the structure are shown in the inset of Fig. 1, where d1 = 1.45 μm, d2 = 4.5 μm, d3 = 2.5 μm, h1 = 150 nm, h2 = 50 nm, g1 = 20 nm, and g2 = 40 nm.

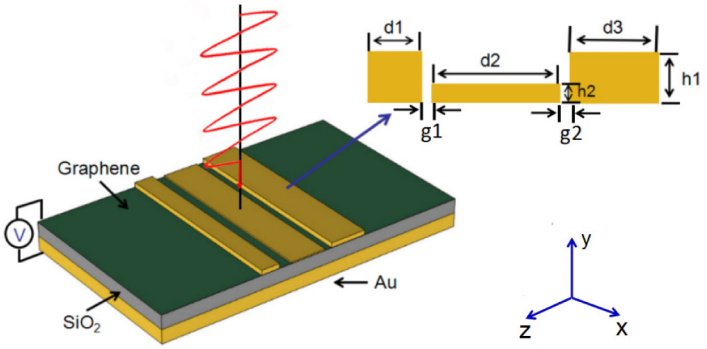

Fig. 1. Schematic of the proposed structure composed of a graphene monolayer and an asymmetric metal nanoantenna positioned atop a 100-nm-thick SiO_2 spacer layer supported by a Au substrate. The inset shows the detailed geometric parameters of the asymmetric nanoantenna.

A plane transverse magnetic (TM) polarization wave (whose magnetic field is perpendicular to the y–z plane) with a wavelength of 6.4 μm is normally incident on the sample plane. Plasmon waves propagated upon application of a voltage V between the graphene sheet and the back-gated Au are investigated by means of the finite element method (FEM). The anisotropicity of graphene can be expressed by means of a diagonal tensor. Graphene's out-of-plane permittivity is set to 2.25, and its in-plane permittivity [25] can be obtained as

$$\varepsilon_g = -\sigma_{g,i} / \varepsilon_0 \omega t + i\sigma_{g,r} / \varepsilon_0 \omega t \quad (1)$$

Optical Materials EXPRESS

where $\sigma_{g,i}$ and $\sigma_{g,r}$ represent the imaginary and real components of the conductivity of graphene (σ_g), and ε_0 and t = 0.33 nm the vacuum permittivity and thickness of graphene, respectively. In the terahertz frequency range, the conductivity of graphene σ_g can be described by means of the following Drude-like expression [26,27]:

$$\sigma_g = i(e^2 E_f / \pi\hbar^2) / (\omega + i\tau^{-1}) \tag{2}$$

Here, E_f and τ represent the Fermi energy level and carrier relaxation time, respectively. Parameters E_f and τ are given as $\hbar v_f(\pi n_g)^{1/2}$ and $\mu E_f / e v_f^2$ [28], respectively, with the Fermi velocity $v_f = 10^6$ m/s and carrier mobility $\mu = 3000$ cm^2/(V·s). In our calculation, the permittivity of the spacer layer SiO_2 is assumed as 2.25, and the optical constants of gold are modeled by the Drude model with a plasma frequency of 1.367×10^{16} rad/s and collision frequency of 6.478×10^{13} rad/s.

3. Results and discussions

Figure 2 shows the cross-sectional view of the y-component of the electric field distribution and power flow distribution for different Fermi energies. Utilizing the gate-voltage dependent optical conductivity of graphene, we can control the propagation characteristics of the SPPs. Figures 2(a)-(c) show the electric field intensity distribution with the increase in the Fermi energy of graphene. As the Fermi energy increases, the electric field intensity in the left side of the structure decreases. At the Fermi energy of 0.5 eV, the electric field intensity in the left region disappears, and thus, the SPP mainly propagates in the right side [Fig. 2(c)]. The corresponding power flow distribution also verifies this result [Fig. 2(d)]. Specifically, the excited SPPs field is highly delocalized, and it extends about four-fifths of incident wavelength to the air layer. Since the wavelength of SPPs is close to the incident light, the excited SPPs are Au-Air interface modes rather than Au-SiO_2 modes. Figure 2(e) characterizes the extinction ratio η as a function of the Fermi energy (here, the extinction ratio η is defined as the ratio of SPP power flow along the right and left sides of the asymmetric antenna). An extinction ratio of η = 61 is achieved at the Fermi energy of 0.5 eV. It is a definitely good performance for a unidirectional SPP launcher with an electrically tunable property. In the following, we would like to unveil the underlying that attributes to this interesting effect

It is well known that a metal nanostrip and a metallic mirror separated by a dielectric spacer can be regarded as a magnetic dipole resonator. Under the magnetic dipole approximation, the radiated field can be defined as [29]

$$E = -\frac{c\mu_0 k_{spp}^2 e^{i\phi}}{4\pi r}(\vec{n}\times\vec{m})\left(1-\frac{1}{ik_{spp}r}\right) \tag{3}$$

where $\vec{m}$ represents the magnetic dipole, $\vec{n}$ the unit vector in the direction of $\vec{r}$ with respect to the position of the dipole, ϕ the radiated phase of the dipole, $k_{spp} = 2\pi/\lambda_{spp}$ the wave vector of SPPs given by [30] $k_{spp} = \frac{2\pi}{\lambda_{in}}\sqrt{\frac{\varepsilon_{eff}\varepsilon_{Au}}{\varepsilon_{eff}+\varepsilon_{Au}}}$ (λ_{in} = vacuum wavelength, λ_{spp} = SPP wavelength, ε_{eff} and ε_{Au} are the effective dielectric constants of dielectric and gold, respectively). If the initial phases of the radiated EM waves excited by LSPs in the two cavities satisfy the following expressions [31]

$$\phi_1(E_f) + d\frac{2\pi}{\lambda_{spp}} = \phi_2(E_f) + (2N+1)\pi \tag{4}$$

$$\phi_2(E_f) + d\frac{2\pi}{\lambda_{spp}} = \phi_1(E_f) + 2N\pi \tag{5}$$

Optical Materials EXPRESS

the radiated EM waves will interfere destructively along the positive direction of the x-axis while interfering constructively along the negative x-direction. This directional propagation of the EM waves leads to the unidirectional propagation of the SPPs. Here, $\varphi_1(E_f)$ and $\varphi_2(E_f)$ denotes the functions of the Fermi energy level of graphene, and the initial phases of $\varphi_1(E_f)$ and $\varphi_2(E_f)$ are different due to the asymmetricity of the device structure. Further, d denotes the distance between the two gaps (g1 and g2), while N denotes an arbitrary integer. Simple manipulation of Eqs. (4) and (5) yields the following expression

$$\phi_1(E_f) - \phi_2(E_f) = \frac{\pi}{2} \tag{6}$$

Thus, unidirectional SPP propagation will occur when the relative phase between the two cavities equals $\pi/2$. Given that the plasmonic resonance of the metallic antenna depends on the geometric size and environment of the cavity (i.e. the gap surrounded by the metallic strip), the resonant phase and frequency of the antenna can be modulated based on the equivalent circuit model [32], when a tunable material such as graphene is introduced in the cavity. To verify that the phase of the cavities is a function of the Fermi energy, the electric field and phase for different Fermi energies in the two cavities are calculated as in Figs. 3(a)-3(d). For the left cavity [Fig. 3(a)], the resonant peak at the wavelength of 6.4 μm is blue-shifted with increase in the Fermi energy. The frequency shift Δω is given by the following formula [32]:

$$\frac{\Delta\omega}{\omega_0} \approx \frac{1}{2\omega_0^4 C_p^2 L_G L} \tag{7}$$

Here, ω_0 denotes the resonance frequency in the absence of graphene, and L and L_G the inductance of the metal pair and graphene, respectively. The inductance of graphene can be expressed as $L_G = -g/\omega^2\varepsilon_0\varepsilon_G t_G = -g/\gamma\omega^2\varepsilon_0 E_f t_G$ (γ denotes a deduced coefficient for simplicity, and g denotes the cavity width), Further, C_p represents the capacitance of the metal pair. The blue-shift of the resonance frequency results from decrease in the graphene inductance L_G because of the injection of external carrier concentration. However, for the right cavity, the inductance of L_G is large due to its larger size. From Eq. (7), we can infer that the resonance frequency in the right cavity [Fig. 3(b)] does not significantly change with increase in the Fermi energy. Thus, the resonant-peak shift affects the resonant phase change in the left cavity. The resonance phases in the left and right cavities are depicted in Figs. 3(c) and 3(d), respectively. As expected, the tuning behavior of the resonant phase agrees well with the simulation results of the electric field in the two cavities. We next plot the phases corresponding to the left and right cavities as a function of the wavelength in Fig. 4 for the Fermi energy of 0.5 eV. The resulting plot confirms that the designed structure meets the phase relationship corresponding to the unidirectional effect. At an incident wavelength of 6.4 μm, a phase difference of $\sim\pi/2$ can be obtained, which is in good agreement with Eq. (6). In addition, by dynamically tuning the Fermi energy of graphene, we can achieve unidirectional SPP propagation over a broadband wavelength range (at incident wavelengths of 5.7-6.7 μm, see Fig. 6 in the Appendix). These results indicate that the unidirectional effect is caused by the interference of the radiated EM waves induced by the two cavities.

Optical Materials EXPRESS

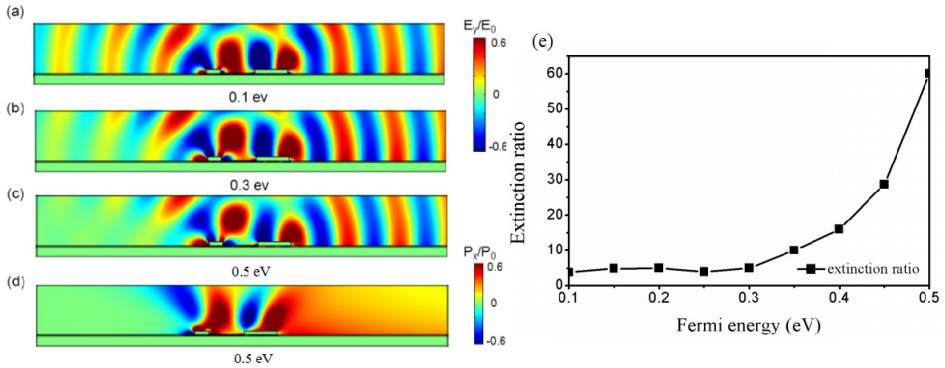

Fig. 2. (a)-(c) The y-component of the normalized electric field distribution at 0.1 eV, 0.3 eV and 0.5 eV, respectively. (d) Plot of the x-component of the power flow distribution at 0.5 eV. (e) Electrically controllable characterization of the extinction ratio as a function of the Fermi energy level.

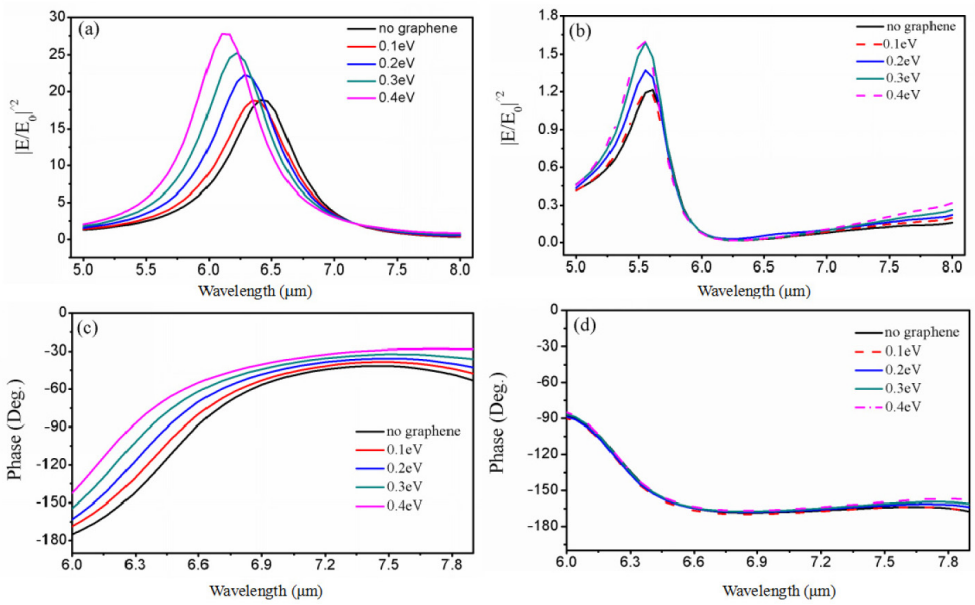

Fig. 3. (a) and (b) Simulated electric field magnitudes at the center of the left and right cavities for varying Fermi energies, respectively. (c) and (d) Dependence of the phases of the left and right cavities on the Fermi energy, respectively.

Optical Materials EXPRESS

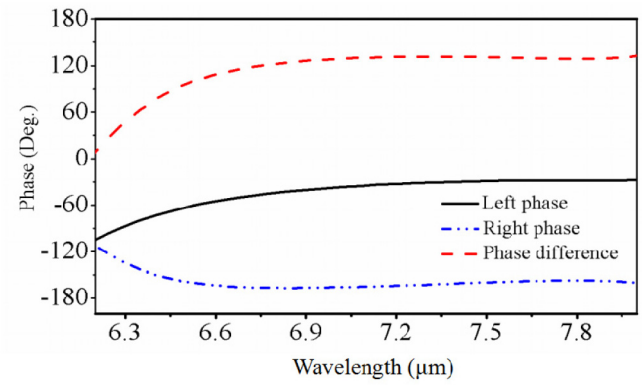

Fig. 4. Phases of the left and right cavities at the Fermi energy of 0.5 eV. The red dashed line indicates the difference in the phase between the two gaps.

Finally, we examine the electric field intensity distribution in the designed structure [Fig. 5(a)]. Figures 5(b) and 5(c) are the electric field intensity distributions with graphene in the left and right cavities, respectively, in both of which the electric field are greatly enhanced compared with those in outside. It is observed that the graphene sheets rightly locate at the strong field region in both cavities that ensures the tunability by changing the graphene's Fermi energy. However, by comparing the field intensity in two cavities, one can find that the left cavity has much stronger field enhancement than the right one, which would reasonably attribute to the different resonant effect according to different cavity parameters. So that, the stronger enhancement of field on graphene, the bigger resonance shift with respect to different Fermi energy (the left cavity), and vise versa (the right cavity), which agree well with the results in Fig. 3(a) and 3(b). Here, the normalized field intensity in the graphene region for left cavity is ~160 V^2/m^2, and the right cavity is ~8.17 V^2/m^2. The tunability of the cavity is proportional to the field intensity in the graphene region. Thus, the left cavity can provide a significantly larger tunable range than the right cavity. Our analyses indicate that the interaction between graphene and the asymmetric antenna gives rise to the directional SPP propagation with tunable capability.

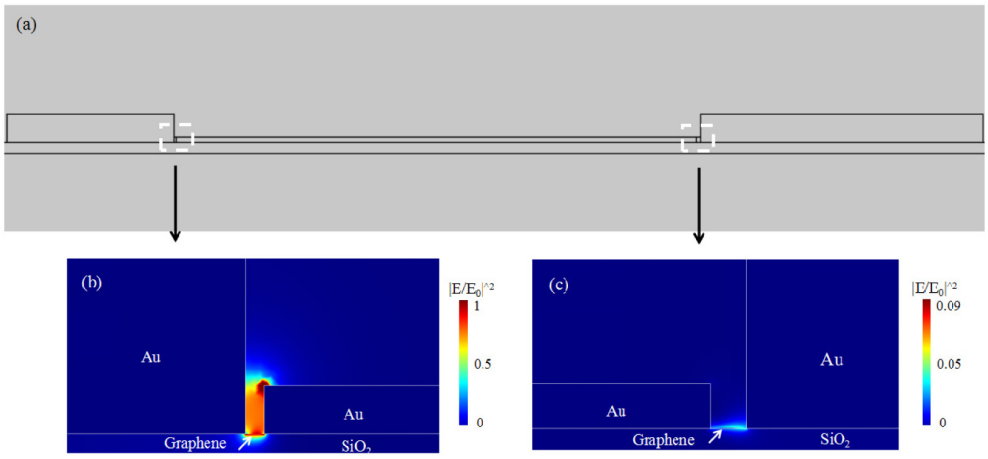

Fig. 5. (a) The cross-sectional views of the structure. (b) and (c) are the simulated electric field intensity distribution with graphene in the vicinity of left and right cavities, respectively. The incident wavelength is 6.4 μm, Fermi energy is 0.2 eV.

Optical Materials EXPRESS

4. Conclusions

In summary, we designed an asymmetric antenna with a graphene sheet on a SiO_2/Au substrate. By applying an external voltage between graphene and Au substrate, we can control the phase of the radiated EM waves, which leads to their constructive or destructive interference along a certain direction. With the development of modern nanofabrication technology, it is possible to fabricate the proposed sample structure by transferring a chemical vapor deposition (CVD)-grown graphene sheet onto SiO_2/Au substrate. The antenna structure and electrode can be fabricated on the graphene sheet by means of electron beam lithography (EBL), electron beam evaporation and lift-off. Such a flexible device can be utilized for diverse plasmonic light sources for future on-chip integration applications [33–36].

Appendix

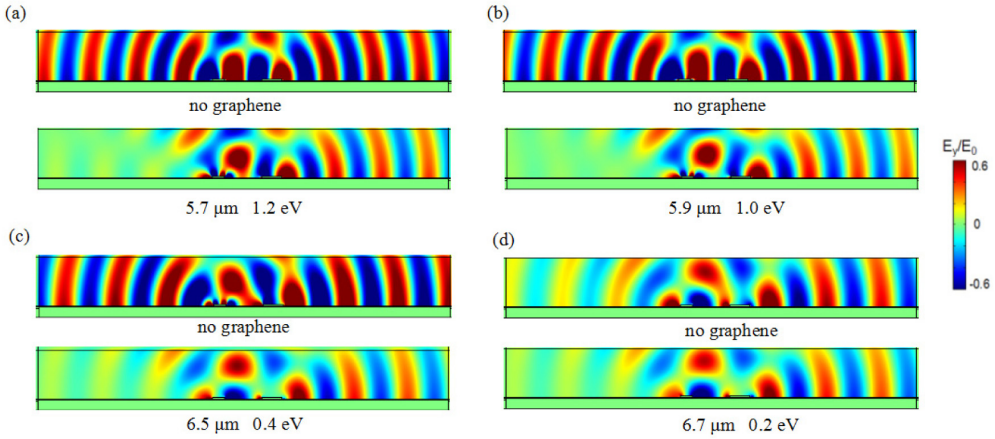

Fig. 6. (a)-(d) The y-component of the normalized electric field distribution at incident wavelength 5.7 μm, 6.5 μm and 6.7 μm, respectively. The unidirectional SPP propagation can be achieved at 1.2 eV, 1.0 eV, 04 eV, and 0.2 eV, respectively.

Funding

This work was supported by the National Natural Science Foundation of China (Nos. 11674167 and 11621091), the Innovation Project of Guangxi Graduate Education (No. YCSZ2016035), the Guangxi Scientific Research and Technological Development Program Topics (No. 1598007-12), the Youth Foundation of Guangxi Normal University (No. 17A4), and the Dengfeng Project B of Nanjing University.